The Impact of Ink and Spray Variables on Catalyst Layer Properties, Electrolyzer Performance, and Electrolyzer Durability

Shaun M. Alia,[1,z] Kimberly S. Reeves,[2] Jefferey S. Baxter,[2] and David A. Cullen[2,*]

[1]*Chemistry and Nanoscience Center, National Renewable Energy Laboratory, Golden, Colorado, United States of America*
[2]*Center for Nanophase Materials Sciences, Oak Ridge National Laboratory, Oak Ridge, Tennessee, United States of America*

In proton exchange membrane-based electrolysis, cell-level performance and durability is affected not only by individual components, but also by how those components are integrated into membrane electrode assemblies. In this study, several ink and ultrasonic spray parameters are evaluated for their effect on catalyst layer properties, electrolyzer performance, and electrolyzer durability. The relative impact of these variables on kinetic and ohmic loss were revealed and linked to catalyst layer morphology. Ionomer loading and dispersion principally affect kinetics and accelerate kinetic loss over time. Catalyst layer uniformity, however, tends to affect ohmic loss, where poor catalyst-transport layer contact adds resistances, increases ohmic loss, and accelerates ohmic loss over time. These efforts to understand catalyst layer formation and the impact of catalyst layer properties on electrolyzer performance and durability aid in the establishment of robust baselines and better inform component development efforts and manufacturing processes. Separating losses and quantifying how losses change during extended operation are also useful as a diagnostics approach to elucidate why suboptimal performance/durability occurs and develop strategies to mitigate loss.

Hydrogen as a chemical commodity has a significant role today in transportation and agriculture. With regards to energy consumption overall, however, hydrogen use has been limited, particularly when produced through electrochemical water splitting due to the high cost. With the emergence of low-cost, intermittent power sources, electrolysis-produced hydrogen has an opportunity for greater use in grid storage and to offload excess energy into other sectors.[1] Load following, i.e. coupling electrolyzers directly with renewable power sources, allows for a dramatic reduction in feedstock cost and can reduce hydrogen production costs to a level comparable to steam methane reforming.[2] Further cost reductions rely on reducing the capital cost, and will likely involve reducing the amount of platinum (Pt) group metals (PGMs) used in electrolyzers.[3–5]

Evaluating degradation is needed as electrolysis shifts to low-cost applications and intermittent inputs, to understand the impact of durability on an electrolyzer's useful lifetime and hydrogen production cost.[6] A variety of past efforts have evaluated aspects of durability, with a focus on the membrane,[7] catalysts,[8–10] transport layers (PTLs),[11–15] and their interfaces. Within catalysis, iridium (Ir)-based nanomaterials are commonly used for the oxygen evolution reaction (OER) in proton exchange membrane (PEM) electrolysis due to reasonable performance and stability.[16–18] Durability studies of OER materials have included fundamental evaluations of dissolution rates, ex situ performance loss, and the development of more active or stable catalysts to improve upon durability or lessen operational (load) requirements.[16,17,19–26] At the device level, durability studies have focused on loss due to constant load and intermittent operation,[8–10,23,27,28] start-stop,[29–31] contaminants,[32] and transport limitations.[33,34]

While the activity and stability of individual components drives device performance and lifetime, how materials are integrated into catalyst layers also has a pronounced effect on electrode properties, performance, and durability. Understanding that impact is critical to provide robust benchmarks for baseline materials and mitigate losses due to suboptimal coatings. This study focuses on catalyst-coated membranes (CCMs) formed through ultrasonic spraying. While spray coating is low throughput and intended for small-scale science, the approach allows for the tuning of a number of variables towards understanding optimal catalyst layer formation, to better inform manufacturing-relevant processes. This work leverages an ongoing program developing accelerated stress tests (ASTs) for PEM electrolyzers, focused on losses associated with intermittent operation.[35]

Experimental

Membrane electrode assemblies (MEAs) were sprayed as CCMs on Nafion 117 with an automated spray station, equipped with an Accumist ultrasonic spray head. Each run sprayed four CCMs, which were placed on top of a thin PTFE layer and a heated vacuum plate. A rubber sheet was used as a gasket to seal the area outside of the spray pattern and ensure vacuum. The head spray path was 6×6 cm and oversprayed the active area to ensure that a loading drop did not occur near the catalyst layer edge. Membranes were vacuumed and heated, and the spray station prepared (calibrated, safety check) prior to forming inks.

Cathode layers were sprayed first with carbon-supported Pt (Pt/HSC, 47 wt% Pt, Tanaka Kikinzoku Kogyo, TEC10E50E) to a loading of 0.1 mg_{Pt} cm^{-2} and an ionomer to carbon ratio of 0.45:1. Catalyst (91.9 mg) was added to distilled deionized water (24.0 ml) and n-propyl alcohol (18.3 ml), and iced for 5 min. Nafion ionomer (109.9 μl, 20 wt%, DE2020) was then added to the ink, which was horn sonicated for 30 s, bath sonicated for 20 min, and horn sonicated for 30 s, all in ice. Following preparation, the ink was loaded into a syringe pump and immediately sprayed at a rate of 0.2 ml min^{-1} onto a Nafion 117 membrane heated to 80 °C. Spraying of the Pt cathodes was based on previous optimization efforts, and a 0.1 mg_{Pt} cm^{-2} loading was used to avoid any impact on cell performance observed at lower catalyst loading ($\leqslant$0.025 mg_{Pt} cm^{-2}).[35]

Anode layers were sprayed next with unsupported Ir oxide (Alfa Aesar, 43396) to a loading of 0.1 mg_{Ir} cm^{-2}. For the Ir oxide used, the catalyst was previously characterized and had a particle size of approximately 5 nm (microscopy), a crystallite size of approximately 7.4 Å (Rietveld refinement of X-ray diffraction), and an electrochemical surface area of 28.7 m^2 g_{Ir}^{-1} (half-cell testing).[23,36,37] Ink composition was varied and included the catalyst concentration (1, 2,
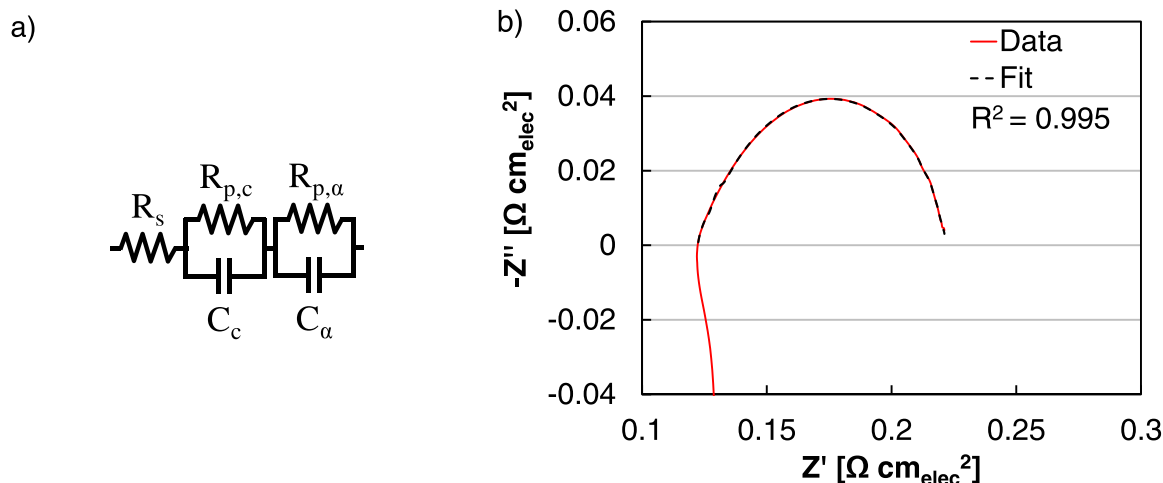
Figure 1. (a) Equivalent circuit model and (b) demonstration of impedance data fitting for the optimum MEA during initial testing. For the optimum MEA, the ink contained 0.2 mg$_{Nafion}$ mg$_{Ir}^{-1}$, at a concentration of 2.75 mg ml^{-1} and a solvent ratio of 0.33 ml$_{Water}$:ml$_{Ink}$, and was sprayed at 0.2 ml min^{-1} onto a membrane heated to 90 °C.

2.75, 3.5, and 5 mg ml^{-1}), solvent ratio (0, 0.25, 0.33, 0.5, 0.6, 0.75, 1 ml$_{Water}$:ml$_{Ink}$), and ionomer loading (0.05, 0.1, 0.2, 0.27, 0.3, 0.6, 0.8 g$_{Nafion}$:g$_{Ir}$, Table I). All Ir inks were prepared with the same procedure, where the catalyst was added to water and n-propyl alcohol, and iced for 5 min. After ionomer was added, the inks were horn sonicated for 30 s, bath sonicated for 20 min, horn sonicated for 30 s (all in ice), and immediately sprayed. For the optimum ink, Ir oxide (113.8 mg) was added to 11.7 ml of distilled deionized water and 23.8 ml of n-propyl alcohol. After 5 min in ice, Nafion ionomer (95.6 μl, 20 wt%, DE2020) was added and the ink horn sonicated for 30 s, bath sonicated for 20 min, and horn sonicated for 30 s, all in ice. After preparation, the ink was immediately sprayed onto a Nafion 117 membrane (cathode catalyst layer previous coated) with a nozzle path speed of 50mm s^{-1}. Spray parameters were varied and included the pump rate (0.1, 0.2, 0.3, 0.4 ml min^{-1}) and the temperature (40 °C, 60 °C, 80 °C, 90 °C, 100 °C, 110 °C, Table I). For the optimum MEA, the ink was sprayed at 0.2 ml min^{-1} onto a membrane heated to 90 °C.

Catalyst layers were sprayed onto Nafion 117 from the same supplier (Ion Power, Inc.) and lot number (1606AE1853). The membranes were kept in the Energy Systems and Integration Facility, Energy Systems Fabrication Laboratory at NREL, which was actively monitored and controlled for temperature at 23.5 °C (23.43 °C–23.56 °C) when the membranes were stored and sprayed. Membranes were sprayed as-received without preconditioning (hydration, boiling in water, or acid exposure) and were sprayed dry to hold the membranes to the heated vacuum plate. During optimum spraying, the membrane was held (vacuum, gaskets) to a heated vacuum plate at 90 °C (3 °C–4 °C decrease through the membrane thickness), except in the spray temperature experiments where the vacuum plate temperature varied 40 °C–110 °C. In all cases, the membrane was fixed to the vacuum plate at temperature prior to equipment safety procedures (automated) and ink formulation (30 min). After the cathode and anode catalyst layers were

sprayed, the CCMs were soaked in water and dried at 50 °C on a vacuum plate. This was done to minimize membrane warping, improve contact and compression uniformity during cell assembly, and limit contact resistances. Vacuuming the CCMs resulted in slight stretching and thinning of the membrane (from 178 to 150 μm on average) and slightly reduced ohmic loss.

Aspects of this process, including preconditioning, ultrasonic spraying, and dry assembly are different from current manufacturing processes. By avoiding a preconditioning/hydration step, we may produce MEAs with lower ionic conductivity and marginally lessen hydrogen crossover. The lower boiling temperature of water at elevation (5674 ft), however, may lessen a conductivity advantage by preconditioning relative to MEA operation (80 °C). Additional hydrating/drying steps were also avoided to prevent further membrane thinning and lower ohmic losses than expected with Nafion 117.

Differences in membrane water content can significantly impact cell performance through stresses in the catalyst layer. In the experiments presented, low catalyst concentration (ink), higher water content (ink), higher pump rate (spray), and lower plate temperature (spray) can all result in excess ink sitting on the membrane surface (Table I). Higher degrees of water adsorption during spraying can create membrane warping and catalyst layer defects that can result in performance and durability differences.

Following CCM fabrication and preparation, X-ray fluorescence (XRF) was completed with a Fischer XDV-SDD energy dispersive XRF spectrometer. Anode/cathode loading confirmations were calculated as the average of 4 measurements with a 30 s exposure. XRF mapping was completed on a 40 × 40 grid (1600 data points) with 30 s exposures (approximately 13.3 h in duration). Cross sections of various CCMs were prepared by diamond-knife ultramicrotomy. Backscattered electron (BSE) images were obtained on a Hitachi S4800 scanning electron microscope (SEM). Bright-field (BF) and high-angle annular dark-field (HAADF) scanning

Table I. Ink and spray variables, including the lower/upper bounds evaluated and optimum values.

Type	Variable	Lower Bound	Upper Bound	Optimum
Ink	Nafion Content	0.05 mg$_{Nafion}$ mg$_{Ir}^{-1}$	0.8 mg$_{Nafion}$ mg$_{Ir}^{-1}$	0.2 mg$_{Nafion}$ mg$_{Ir}^{-1}$
Ink	Catalyst Concentration	1 mg ml^{-1}	5 mg ml^{-1}	2.75 mg ml^{-1}
Ink	Solvent Ratio	0 ml$_{Water}$:ml$_{Ink}$	1 ml$_{Water}$:ml$_{Ink}$	0.33 ml$_{Water}$:ml$_{Ink}$
Spray	Pump Rate	0.1 ml min^{-1}	0.4 ml min^{-1}	0.2 ml min^{-1}
Spray	Temperature	40 °C	110 °C	90 °C

transmission electron microscopy (STEM) images along with energy dispersive X-ray spectroscopy (EDS) spectrum images were taken on a FEI Talos operated at 200 keV.

MEAs with an active area of 25 cm^2 were assembled using Fuel Cell Technologies hardware, carbon PTLs (Toray) and flow fields (Fuel Cell Technologies) at the cathode, and Pt-coated titanium PTLs and flow fields (Giner Inc.) at the anode. MEA testing was completed with Greenlight test stands, using a dry cathode with no applied back pressure, a water flow of 0.3 l min^{-1} at the anode, and a cell temperature of 80 °C. Cell conditioning was completed with holds at 0.2 A cm^{-2} for 1 h, 1 A cm^{-2} for 1 h, 2 V for 30 min, 1.7 V for 2 h, and 2 V for 30 min Polarization curves were taken galvanostatically, anodically then cathodically, with 5 min step durations.

Following performance evaluations, cyclic voltammograms (0.025–1.3 V) were taken along with impedance spectra (1 Hz–100 kHz) at each current density (or potential) used in the polarization curves. Impedance spectra at 0.2 A cm^{-2} were fit to a modified Randles cell equivalent circuit model to monitor the solution resistance (R$_s$, HFR), polarization resistances (R$_{p,\alpha}$, R$_{p,c}$), and capacitances (C$_\alpha$, C$_c$, Fig. 1).[38–40] The polarization resistance (R$_{p,c}$) and capacitance (C$_c$) associated with the shoulder at low Z' were consistent (R$_{p,c}$ = 0.002 Ω cm^2, C$_c$ = 24.1 mF cm^{-2}) and did not significantly change with variations to the ink composition, spray parameters, or extended operation. The solution resistance (R$_s$), polarization resistance (R$_{p,\alpha}$), and capacitance (C$_\alpha$), however, varied significantly and were presented as tabulated values throughout MEA testing. Polarization curves and diagnostics were used to examine the sources of suboptimal performance and how these nonidealities changed over time. Ohmic loss was evaluated from the difference between polarization curves, uncorrected and corrected for high frequency resistance (HFR). Transport loss was evaluated from the difference between the polarization curve corrected for HFR and kinetic performance (exchange current density, Tafel

slope). Kinetics were evaluated from the polarization curves corrected for ohmic and transport loss.

Durability testing was completed using previously developed ASTs, 31.5 k square-wave cycles (30 s at 1.45 V, 30 s at 2 V).[9] These protocols focused on catalyst layer and interfacial deterioration associated with low catalyst loading and intermittent operation. Particularly low loading for the anode catalyst (0.1 mg$_{Ir}$ cm^{-2}) was needed to accelerate loss observations so that experiments could be completed in a reasonable timeframe (525 h). Cycles based on potential were used to focus on the loss mechanism, since Ir dissolution and catalyst layer degradation were based on potential exposure. The durability test used addresses catalyst layer degradation due to intermittent input and is not a current field test replacement since: the test focuses on a single degradation mechanism; and the majority of low temperature electrolyzers in the field use a constant load as opposed to load following renewable power. Other degradation mechanisms impact the catalyst layers (crossover, contaminants, defects), membrane (back pressure and temperature cycling, creep, water starvation), and transport layers/separators (defects, coating continuity and thickness). Additionally, catalyst layer composition and fabrication impact the degradation of other components and interfaces, including the transport layer (exposure) and catalyst-membrane interface (tearing). These differences can also potentially affect catalyst layer degradation through other processes, including hydrogen crossover (catalyst redox), contaminants and defects, and different accelerated stress tests are needed to examine these mechanisms. Several of these mechanisms have been studied elsewhere; others (membranes, transport layers, combined processes), including ASTs related to future intended operation, will be addressed in the near future.[35,41]

For reproducibility, each experiment sprayed four oversized 25 cm^2 MEAs to keep the sprayed area constant. Of these four, two were tested for performance/durability, and another saved for characterization. If the performance was near the optimum, a third
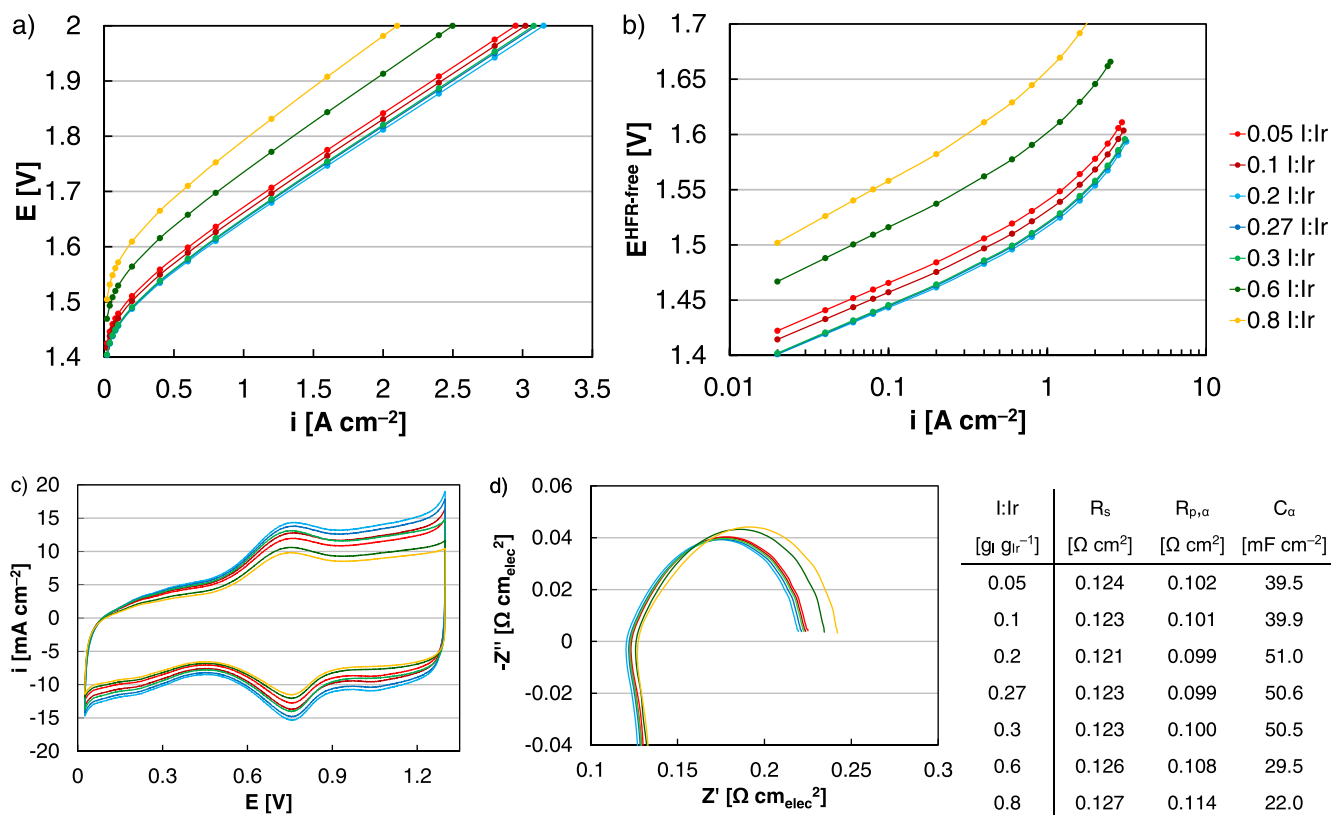

Figure 2. (a) Polarization curves, (b) HFR-corrected Tafel plots, (c) cyclic voltammograms, and (d) impedance spectra of MEAs sprayed with varying solid concentration in the anode catalyst layer ink at beginning of life. MEAs consisted of Ir oxide anodes and Pt/HSC cathodes with loadings of 0.1 mg$_{Ir,Pt}$ cm^{-2}, and were operated at 80 °C.

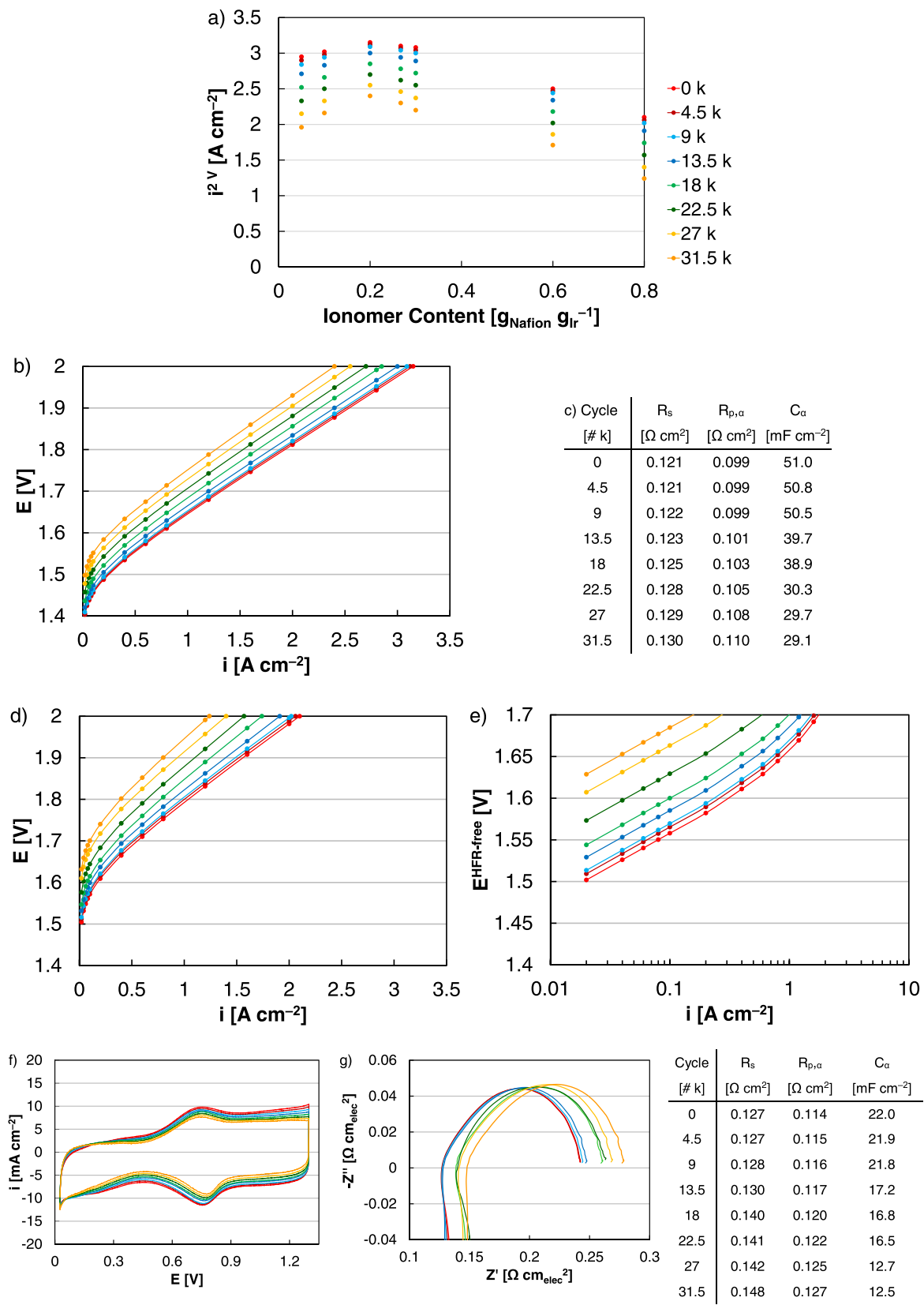| I:Ir	R$_s$	R$_{p,\alpha}$	C$_\alpha$
[g$_I$ g$_{Ir}^{-1}$]	[Ω cm^2]	[Ω cm^2]	[mF cm^{-2}]
0.05	0.124	0.102	39.5
0.1	0.123	0.101	39.9
0.2	0.121	0.099	51.0
0.27	0.123	0.099	50.6
0.3	0.123	0.100	50.5
0.6	0.126	0.108	29.5
0.8	0.127	0.114	22.0

Figure 3. (a) Current density at 2 V as a function of AST cycle count for MEAs sprayed with varying ionomer loading in the anode catalyst layer. (b) Polarization curves and (c) fits to impedance spectra of MEAs sprayed with an ionomer to catalyst ratio (I:Ir) of 0.2 mg_{Nafion} mg_{Ir}^{-1} as a function of AST cycle count. (d) Polarization curves, (e) HFR-corrected Tafel plots, (f) cyclic voltammograms, and (g) impedance spectra of MEAs sprayed with an ionomer to catalyst ratio (I:Ir) of 0.8 mg_{Nafion} mg_{Ir}^{-1} as a function of AST cycle count. MEAs consisted of Ir oxide anodes and Pt/HSC cathodes with loadings of 0.1 $mg_{Ir,Pt}$ cm^{-2}, and were operated at 80 °C.

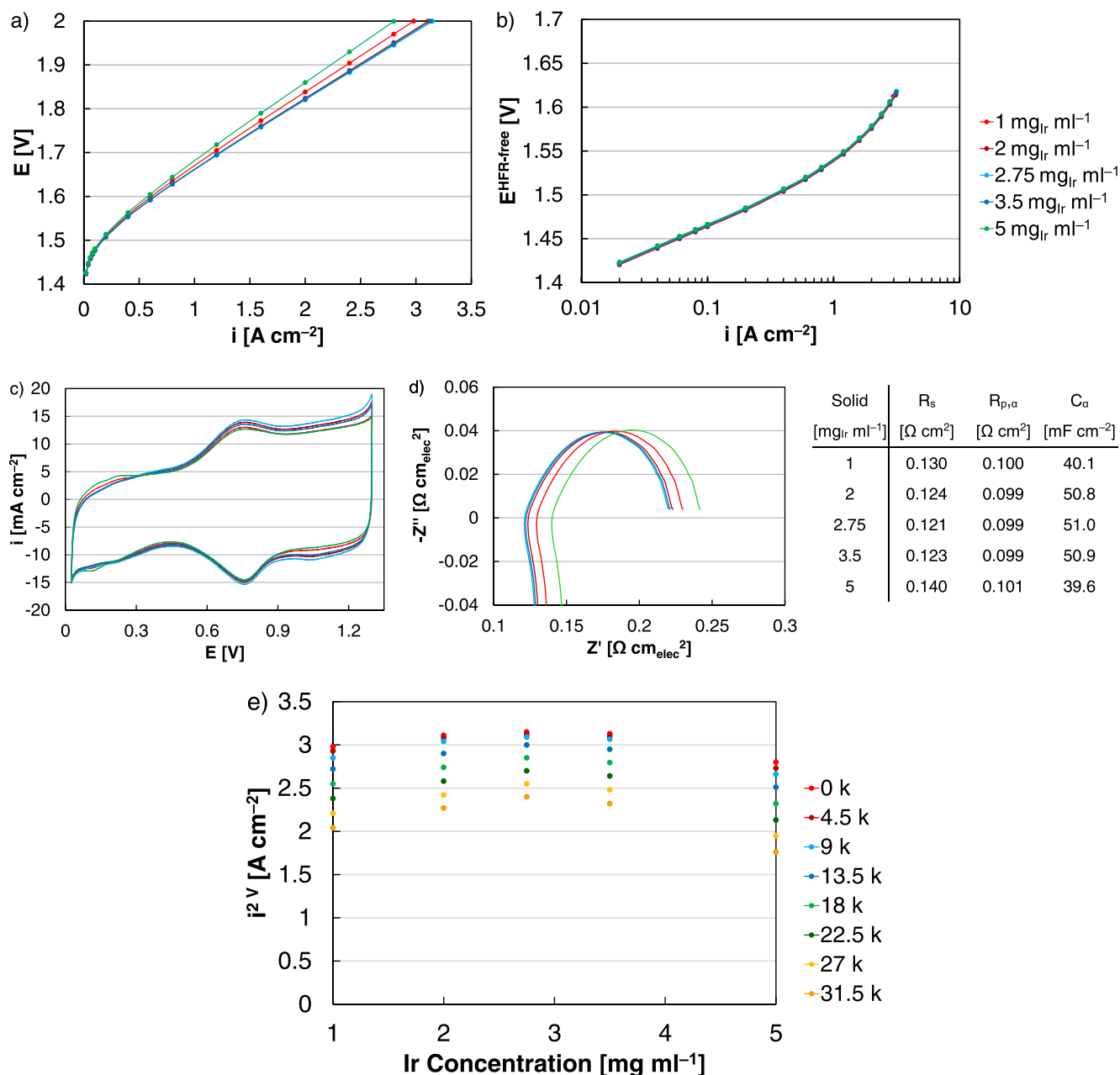| Solid	R_s	$R_{p,\alpha}$	C_α
[mg$_{Ir}$ ml^{-1}]	[Ω cm^2]	[Ω cm^2]	[mF cm^{-2}]
1	0.130	0.100	40.1
2	0.124	0.099	50.8
2.75	0.121	0.099	51.0
3.5	0.123	0.099	50.9
5	0.140	0.101	39.6

Figure 4. (a) Polarization curves, (b) HFR-corrected Tafel plots, (c) cyclic voltammograms, and (d) impedance spectra of MEAs sprayed with varying solid concentration in the anode catalyst layer ink at beginning of life. (e) Current density at 2 V as a function of AST cycle count for MEAs sprayed with varied solid concentration in the anode catalyst layer ink. (f) Polarization curves, (g) HFR-corrected Tafel plots, (h) cyclic voltammograms, and (i) impedance spectra of MEAs sprayed with a solid concentration in the anode catalyst layer ink of 5 mg$_{Ir}$ ml^{-1} as a function of AST cycle count. MEAs consisted of Ir oxide anodes and Pt/HSC cathodes with loadings of 0.1 mg$_{Ir,Pt}$ cm^{-2}, and were operated at 80 °C.

MEA was included in testing to ensure that the optimum was accurately reported. Within individual experiments, performance/ durability were reproducible (within 4 mV at each current density, average reported), provided that the MEAs were: sprayed at the same time, with the same membrane/catalyst (supplier, lot); and tested with the same hardware (transport layers, configuration), with identical temperature controls, similar water conductivities, and minimal shutdowns or excursions. MEA reproducibility issues, however, clearly occur when sprayed at different times or with different processes. For ultrasonic spraying specifically, differences in sonication monitoring and the time between the end of sonication and the beginning of spraying can affect catalyst layer properties and MEA performance. In this manuscript, all spraying was completed by the same user with efforts taken to limit

processing variability and the duration between sonication and spraying (<3 min).

Results and Discussion

Several factors that can impact catalyst layer properties, MEA performance, and MEA durability were evaluated in this study. These variables were categorized based on whether tuning occurred during ink formulation or electrode spraying. Ink variables included the ionomer content, solid concentration, and solvent ratio; spray parameters included the pump rate and drying temperature (Table I). These examinations used in situ testing, cell diagnostics, and ex situ characterization to separate losses, describe how losses changed over time, and assess why these losses occurred.
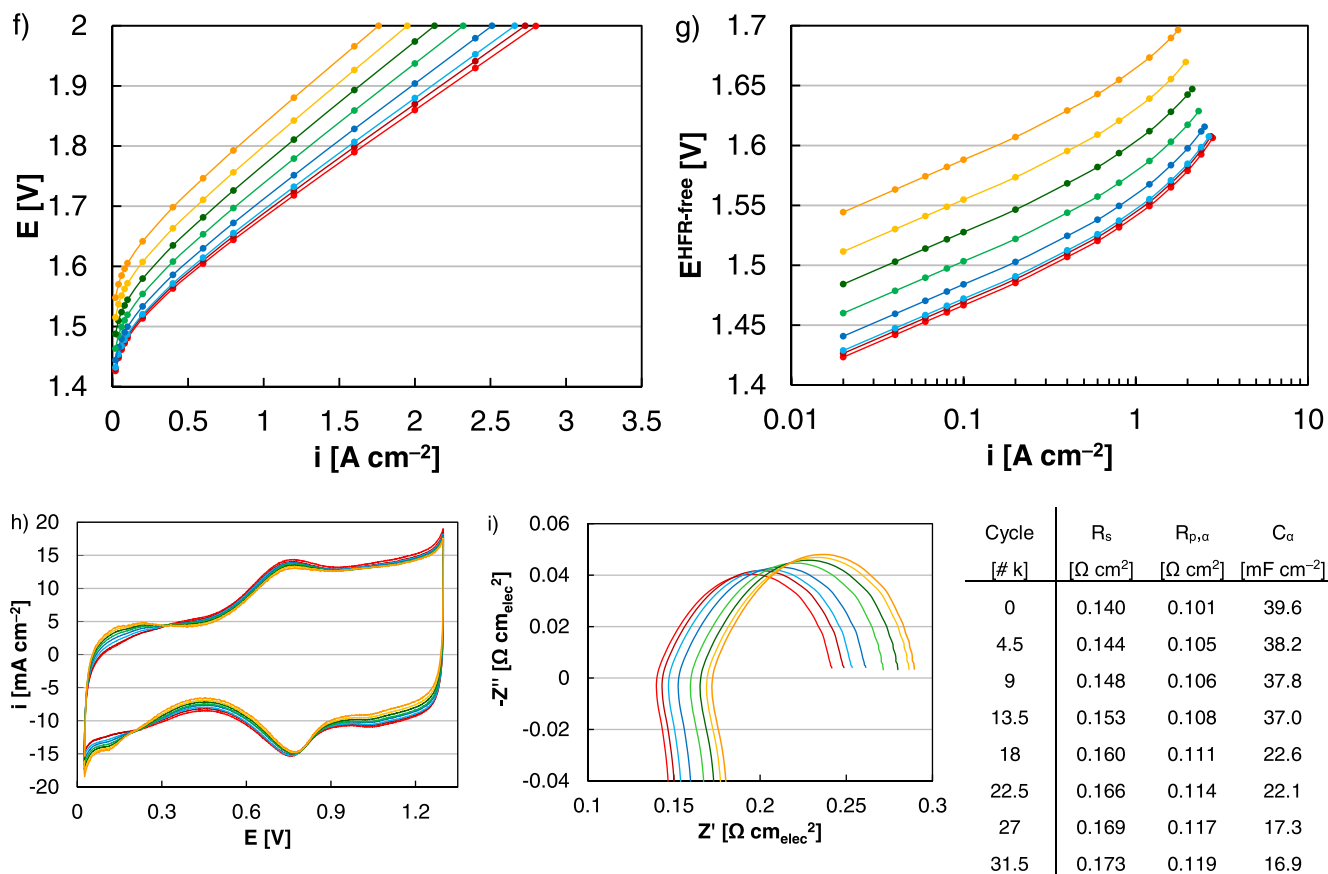
Figure 4. (Continued.)

Durability testing focused on catalyst layer and interfacial degradation, and used previously developed protocols focused on the effect of low loading and intermittent operation to accelerate degradation.[9] Specifically, durability testing throughout these experiments consisted of 31,500 square-wave cycles with 30 s at 1.45 V and 30 s at 2 V. In previous durability studies, large kinetic losses were observed and corresponded to Ir dissolution at elevated potential, catalyst layer thinning, and pore loss (slight decreases in porosity and pore diameter).[35] More aggressive operation led to tearing at the catalyst/membrane interface, which manifested as ohmic loss (slight transport increases) potentially due to interfacial deterioration adding contact resistances.[35] In this study, ink and spray parameters were tuned to find an optimum in cell performance/ durability with standard material sets and to assess the impact of these parameters on catalyst layer properties and MEA performance/ durability.

Ink variables.—The first variable explored was the anode ionomer loading, with a relatively large range of values (0.05–0.8 mg_{Nafion} mg_{Ir}^{-1}). It was the only variable to impact the catalyst to ionomer ratio, and was unique in that it produced a wide range of performances resulting in primarily kinetic changes. At low ionomer amounts (0.05–0.3 mg_{Nafion} mg_{Ir}^{-1}), the resulting MEA polarization curves were similar, and near the optimum (0.15–0.3 mg_{Nafion} mg_{Ir}^{-1}) were nearly identical (Fig. 2a). Higher ionomer amounts adversely affected kinetics, and corresponded to small increases in the polarization resistance and thinning of the cyclic voltammogram capacitance (Figs. 2b–2d). Slower kinetics were likely due to excess ionomer adsorbing onto Ir surfaces and limiting access to Ir sites.[21] Although capacitance is inherently not surface sensitive, the cyclic voltammogram shape and intensity appeared to be generally reflective of Ir oxide accessibility in the catalyst layer, and cyclic

voltammogram thinning at high ionomer content (0.6–0.8 mg_{Nafion} mg_{Ir}^{-1}) may have been due to Ir isolation (Fig. 2c). Slightly higher transport losses were also observed at high ionomer content, and excess ionomer may inhibit oxygen/water diffusion.[42] Additionally, higher ohmic loss was found with higher ionomer content, although the range of high frequency resistance values (0.121–0.127 Ω cm^2) was smaller than any other variable (ink or spray) evaluated. Increased ohmic losses at higher ionomer content could be due to differences in current distribution throughout the catalyst layer with reactions increasingly occurring near the interfaces. Higher degrees of catalyst-ionomer segregation could also potentially increase the high frequency resistance if excess ionomer grouped at the membrane-catalyst layer interface, although obvious ionomer grouping toward interfaces was not found in microscopy. From these results, it becomes clear that tuning the ionomer content is a necessary first step to achieving reasonable MEA performance. Some amount of ionomer is needed in the catalyst layer to ensure contact between active sites and the membrane; excess ionomer, however, may block and isolate sites and at high content, slightly inhibit water transport and add resistances.

In durability testing, the ionomer content altered the performance loss rate, from 3.4 (0.2 mg_{Nafion} mg_{Ir}^{-1}) to 5.1 μV cycle^{-1} (0.8 mg_{Nafion} mg_{Ir}^{-1}, Fig. 3a). Of the variables studied, however, altering the ionomer loading resulted in a relatively small change in the performance loss rate. Losses were primarily due to decreasing kinetics, corresponded to slight changes in cyclic voltammograms (thinning) and impedance spectra (increasing polarization resistance), and were consistent with previous findings where loss was attributed to Ir dissolution and catalyst layer degradation (Figs. 3b, 3c).[9] At or near the optimum ionomer content (0.05–0.3 mg_{Nafion} mg_{Ir}^{-1}), small transport and ohmic changes were found. At high ionomer content, however, these losses increased and accounted for
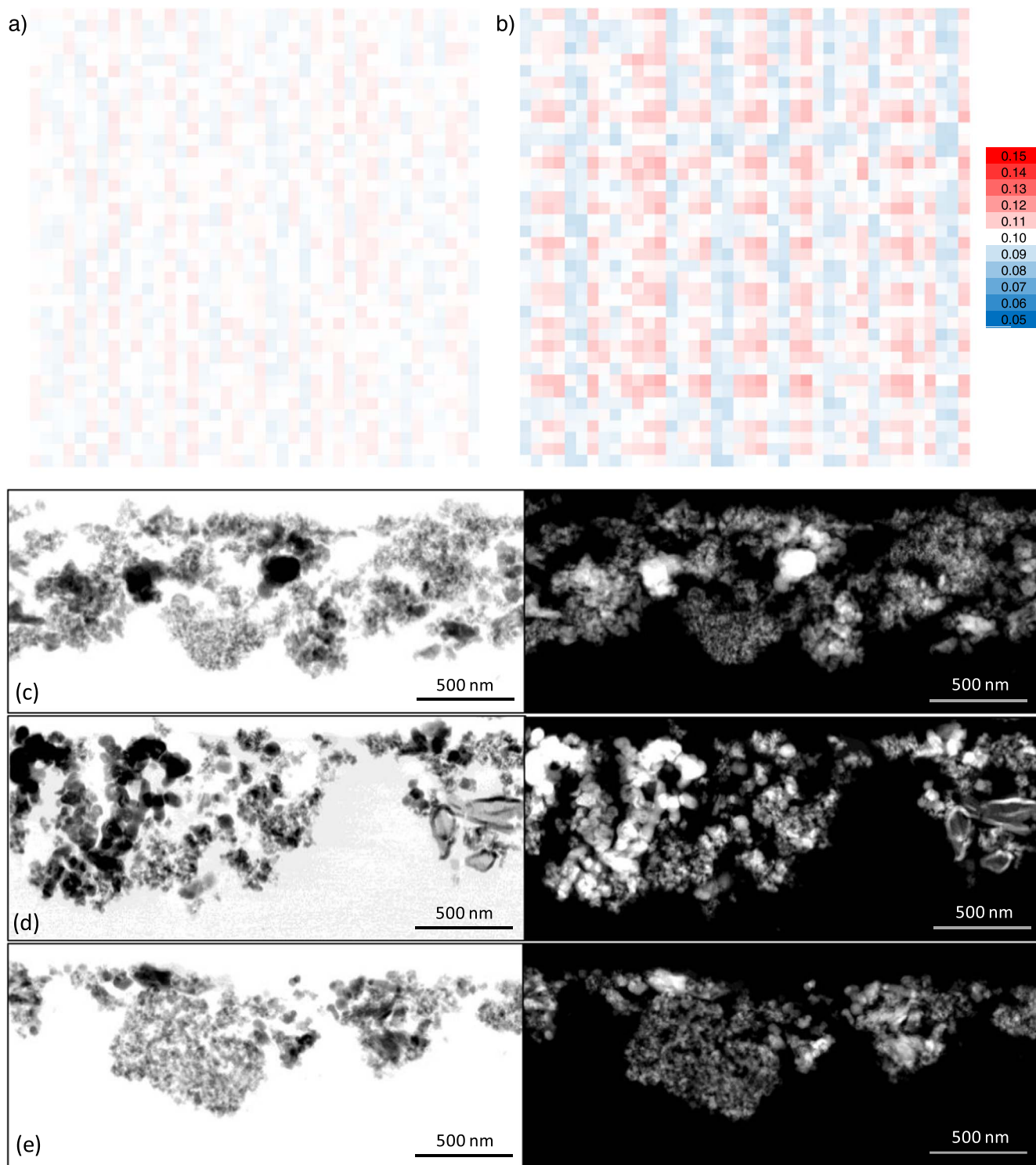
Figure 5. XRF mapping of MEAs sprayed with a solid concentration in the anode catalyst layer of (a) 2.75 and (b) 5 mg_{Ir} ml^{-1}. BF- and HAADF-STEM images of cross-sectioned anode catalyst layers sprayed for (c) optimal performance (solid concentration 2.75 mg_{Ir} ml^{-1}, solvent ratio of 0.33 ml_{H2O} ml_{Ink}^{-1}), (d) high solid concentration (solid concentration 5 mg_{Ir} ml^{-1}, solvent ratio of 0.33 ml_{H2O} ml_{Ink}^{-1}), and (e) high solvent ratio (solid concentration 2.75 mg_{Ir} ml^{-1}, solvent ratio of 0.6 ml_{H2O} ml_{Ink}^{-1}).

the overall change in loss rate (3.4–5.1 μV $cycle^1$, Figs. 3d–3g). Of interest was that higher ionomer content resulted in slightly higher durability losses even though the catalyst layers contained the same amount of Ir and were exposed to the same stressor (square wave, 1.45–2 V). These results indicate that when starting from a lower initial performance and with access to a fewer number of Ir sites,

extended operation may accelerate interfacial tearing and result in the earlier onset of transport and ohmic loss (Fig. 3g).

Following ionomer loading, the second variable explored was the anode solid concentration (i.e. the ratio of Ir oxide catalyst to solvent), where the impact on cell performance was primarily ohmic. Modifications to the solid concentration kept the ionomer content
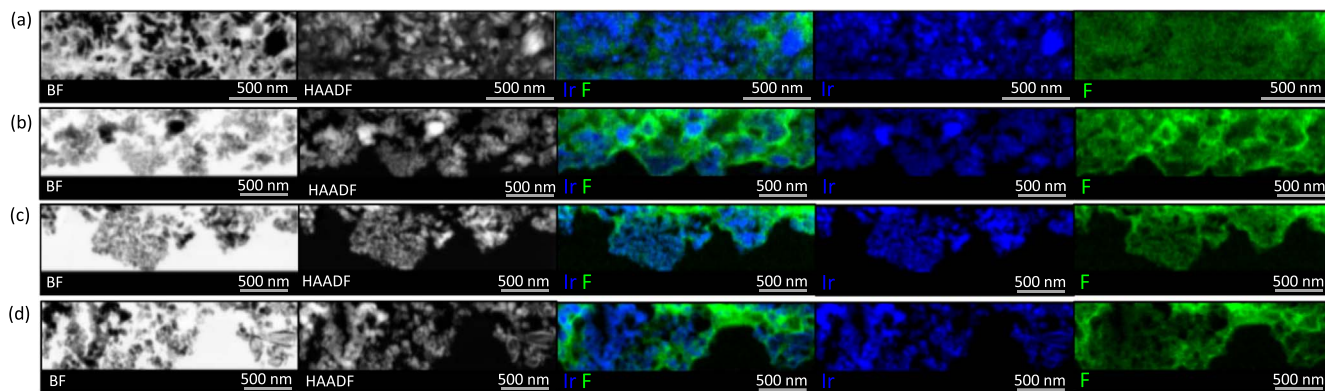
Figure 6. BF- and HAADF-STEM images with EDS spectrum images (Ir, F) of cross-sectioned anode catalyst layers sprayed for (a) optimal performance (ionomer content 0.2 mg_I mg_{Ir}^{-1}, solid concentration 2.75 mg_{Ir} ml^{-1}, solvent ratio of 0.33 ml_{H2O} ml_{Ink}^{-1}), (b) high ionomer content (ionomer content 0.8 mg_I mg_{Ir}^{-1}, solid concentration 2.75 mg_{Ir} ml^{-1}, solvent ratio of 0.33 ml_{H2O} ml_{Ink}^{-1}), (c) high solid concentration (ionomer content 0.2 mg_I mg_{Ir}^{-1}, solid concentration 5 mg_{Ir} ml^{-1}, solvent ratio of 0.33 ml_{H2O} ml_{Ink}^{-1}), and (d) high solvent ratio (ionomer content 0.2 mg_I mg_{Ir}^{-1}, solid concentration 2.75 mg_{Ir} ml^{-1}, solvent ratio of 0.6 ml_{H2O} ml_{Ink}^{-1}).
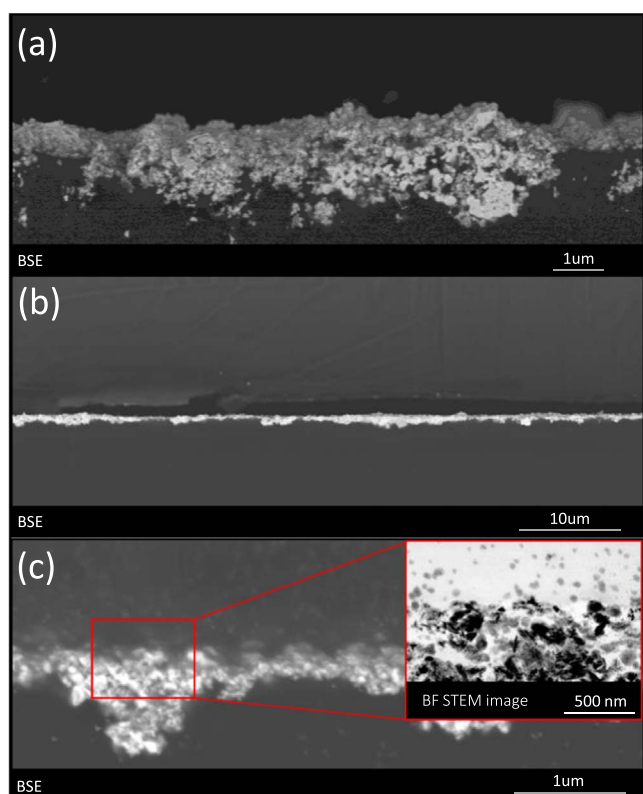

Figure 7. BSE-SEM images of cross-sectioned anode catalyst layers sprayed demonstrating (a) catalyst layer persistence (high ionomer content MEA, ionomer content 0.8 mg_I mg_{Ir}^{-1}, solid concentration 2.75 mg_{Ir} ml^{-1}, solvent ratio of 0.33 ml_{H2O} ml_{Ink}^{-1}), (b) interfacial tearing (optimal MEA, ionomer content 0.2 mg_I mg_{Ir}^{-1}, solid concentration 2.75 mg_{Ir} ml^{-1}, solvent ratio of 0.33 ml_{H2O} ml_{Ink}^{-1}), and (c) Ir migration (high solvent ratio, ionomer content 0.2 mg_I mg_{Ir}^{-1}, solid concentration 2.75 mg_{Ir} ml^{-1}, solvent ratio of 0.6 ml_{H2O} ml_{Ink}^{-1}). MEAs consisted of Ir oxide anodes and Pt/HSC cathodes with loadings of 0.1 $mg_{Ir,Pt}$ cm^{-2}, and were operated at 80 °C. ASTs consisted of square-wave cycles, 30 s at 1.45 V followed by 30 s at 2 V.

(0.2 mg_{Nafion} mg_{Ir}^{-1}) constant, and changes to this variable clearly affected the quality of the ink dispersion and the time required to spray electrodes. High concentrations of Ir catalyst appeared to settle out of suspension (visual catalyst settling, surrounded by clear or nearly clear solvent) at a faster rate. At low concentrations, however, the time to spray electrodes significantly increased (from 26 min at

5 mg_{Ir} ml^{-1} to 130 min at 1 mg_{Ir} ml^{-1}, for 4 × 25 cm^2) and Ir agglomeration in the spray line was observed, particularly near the end of spraying. While these concerns may be partially mitigated once the ink reached the ultrasonic spray head, the solid concentration clearly affected performance (Fig. 4a). Changes to the solid concentration had a small impact on kinetics (exchange current density), polarization resistances (0.099–0.101 Ω cm^2 at 1.2 A cm^{-2}), and capacitances in cyclic voltammograms (Figs. 4b–4d). The performance differences were primarily ohmic, where the HFR varied from 121 $m\Omega$ cm^2 (2.75 mg_{Ir} ml^{-1}) to 139 $m\Omega$ cm^2 (5 mg_{Ir} ml^{-1}, Fig. 4d). High HFR values corresponded to changes in the cyclic voltammograms at low potential, where inflections consistent with hydrogen underpotential deposition were found and suggested increased interaction with the Pt-coating on the PTL (Fig. 4c).

Ex situ characterization of the catalyst layers was used to investigate possible causes for lower performance, higher ohmic loss, and increased Pt features in cyclic voltammograms. While optimum concentrations resulted in relatively uniform Ir layer thicknesses, high concentration (5 mg_{Ir} ml^{-1}) produced catalyst layers with nonuniformities. The variation was apparent with XRF mapping, where the Ir loading (0.101 ± 0.006 mg_{Ir} cm^{-2}) had minimum and maximum values of 0.117 and 0.089 mg_{Ir} cm^{-2} (Figs. 5a, 5b). As a comparison, XRF mapping of the optimum MEA anode (2.75 mg_{Ir} ml^{-1}, 0.101 ± 0.002 mg_{Ir} cm^{-2}) had minimum and maximum values of 0.095 and 0.105 mg_{Ir} cm^{-2}. Additionally, microscopy revealed nonuniformities at finer spatial resolution (Figs. 5c–5e). Comparing the catalysts layers formed at the optimal (2.75 mg_{Ir} ml^{-1}) and high concentration (5 mg_{Ir} ml^{-1}), relatively consistent layer thickness were found in the optimal anode (650–750 nm); large variability, however, was found with high concentration where the thickness varied significantly (150 nm to 1 μm) even within a single imaging spanning 6 μm. From these results, nonuniformities may add slight resistances through poor catalyst-PTL interfacial contact, increasing the ohmic loss and accounting for lower cell performance. At high solid concentration, Pt characteristics in cyclic voltammograms associated with hydrogen underpotential deposition (proton adsorption, desorption) may also be due to nonuniformities, where very thin portions of the catalyst layer allow greater access to the Pt-coating on the PTL.

In addition to catalyst layer thickness variations, changes in porosity and catalyst-ionomer integration can also impact performance. Although not excessively different on average, the catalyst layer thicknesses of suboptimal coatings appeared thinner in places (Figs. 5c–5e) while at the same Ir loading, suggesting that differences in porosity may exist. For the high solid concentration catalyst layer, the Ir particles also appeared to agglomerate more frequently (denser sections, higher contrast), which may impact site
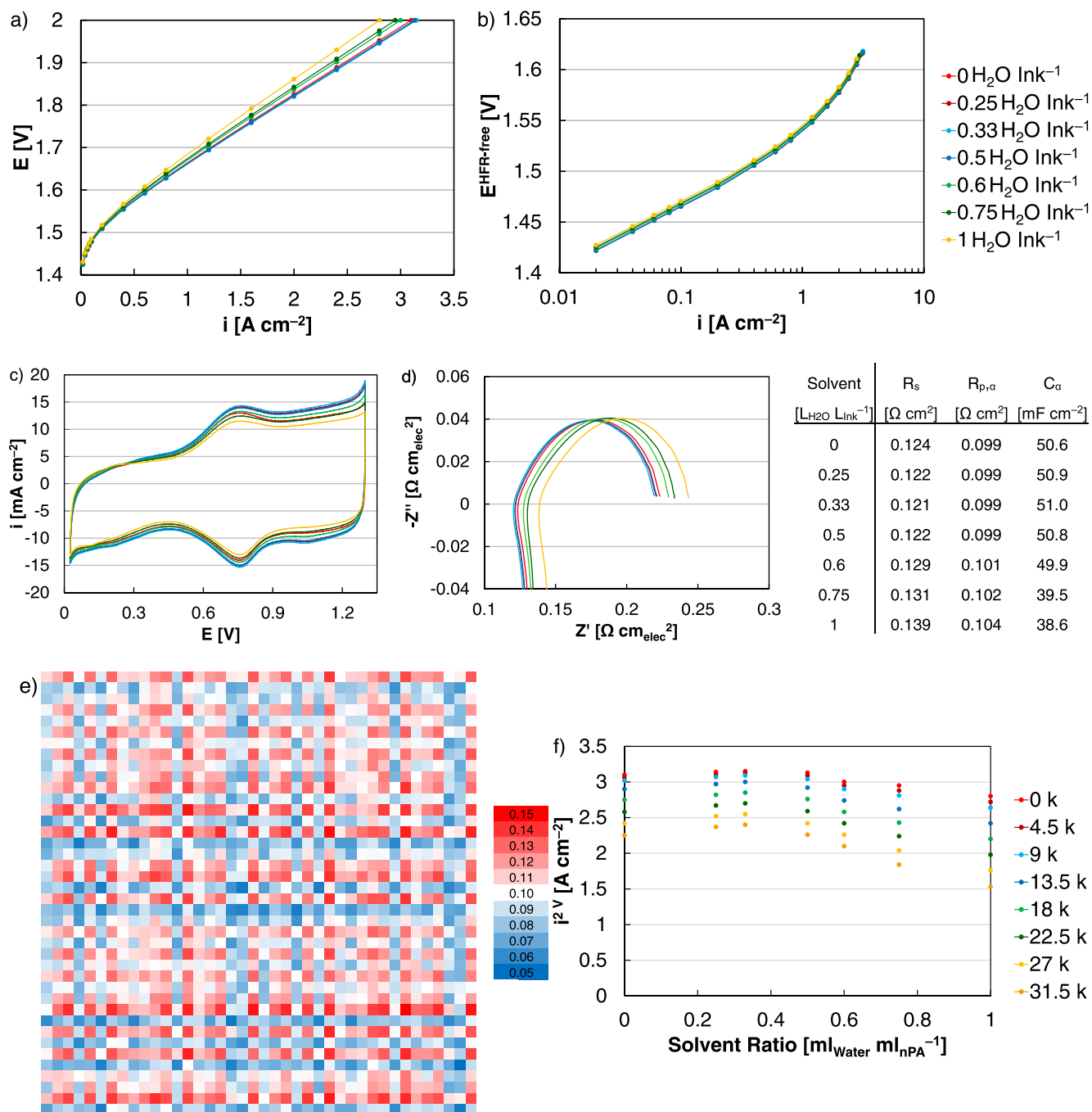
Figure 8. (a) Polarization curves, (b) HFR-corrected Tafel plots, (c) cyclic voltammograms, and (d) impedance spectra of MEAs sprayed by varying the solvent ratio in the anode catalyst layer ink at beginning of life. (e) XRF mapping of MEAs sprayed with a solvent ratio in the anode catalyst layer ink of 1 ml$_{Water}$ ml$_{Ink}^{-1}$. (f) Current density at 2 V as a function of AST cycle count for MEAs sprayed with different solvent ratios in the anode catalyst layer ink. (g) Polarization curves, (h) HFR-corrected Tafel plots, (i) cyclic voltammograms, and (j) impedance spectra of MEAs sprayed with a solvent ratio in the anode catalyst layer ink of 1 ml$_{Water}$ ml$_{Ink}^{-1}$ as a function of AST cycle count. MEAs consisted of Ir oxide anodes and Pt/HSC cathodes with loadings of 0.1 mg$_{Ir,Pt}$ cm^{-2}, and were operated at 80 °C.

access and diffusion (Fig. 5d). Elemental maps for Ir and fluorine extracted from STEM-EDS spectrum images of cross-sectioned MEAs was used to evaluate catalyst-ionomer interaction, where reasonable incorporation was generally found. For the optimal anode, a consistent fluorine signal was found throughout the catalyst layer with relatively few large void spots (Fig. 6a). Higher ionomer content eliminated any void space and resulted in patches of high fluorine signal, indicating that excess ionomer may not spread uniformly and may contaminate sites heterogeneously (Fig. 6b). In contrast, high solid concentration appeared to slightly increase the

frequency of ionomer void spaces and patches of ionomer without catalyst were found (Fig. 6c). These results indicate that high solid concentration may result in poorer catalyst-ionomer integration, although significant differences in kinetic performance were not found. In addition to differences in catalyst layer formation, water-heavy inks and processing conditions that increase the quantity/time solvent sits on the membrane can result in membrane swelling that creates catalyst layer defects. Although obvious defects were not found in microscopy, strain in the catalyst layer or at the catalyst layer/membrane interface could also contribute to higher losses
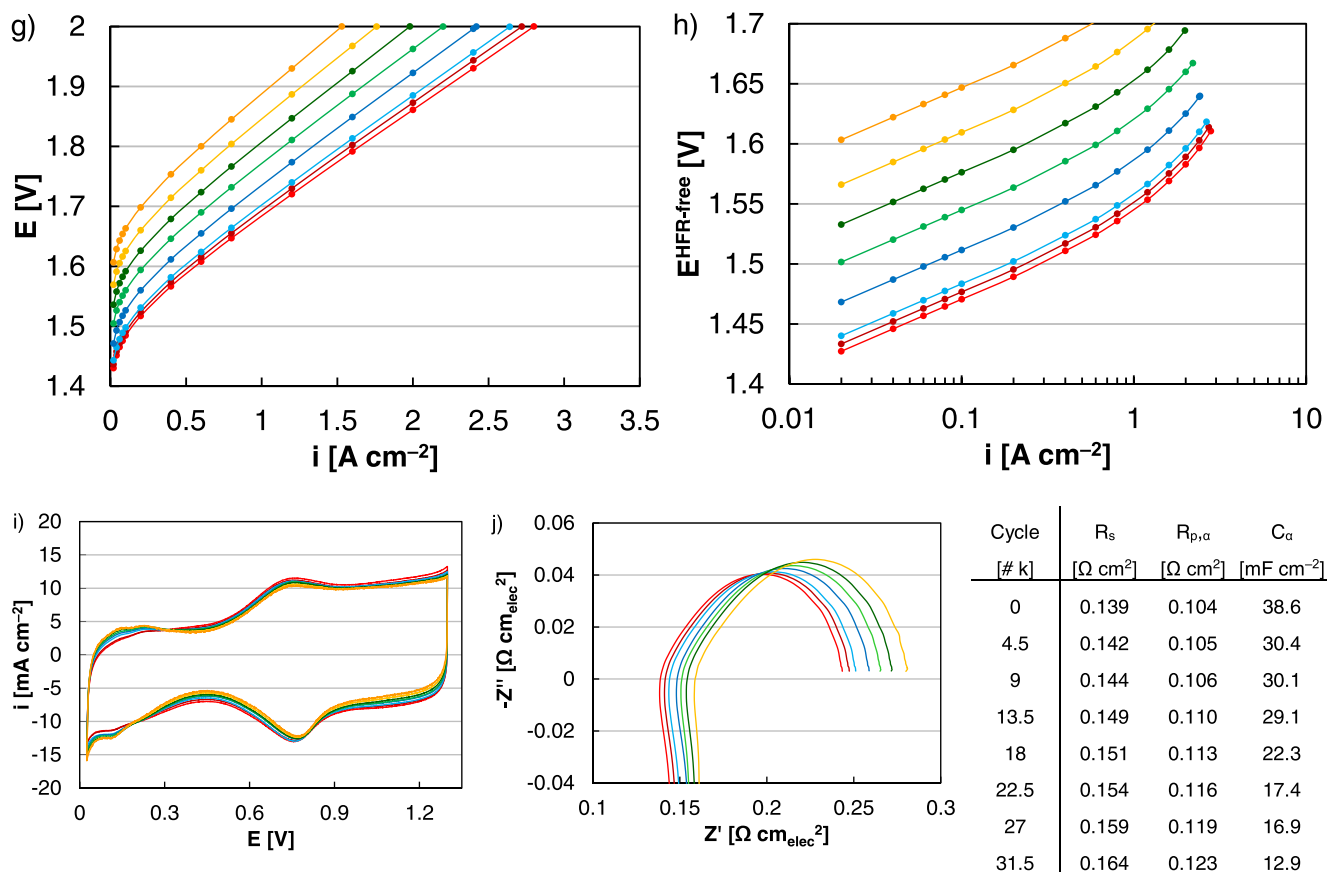
Cycle	R_s	$R_{p,\alpha}$	C_α
[# k]	[Ω cm^2]	[Ω cm^2]	[mF cm^{-2}]
0	0.139	0.104	38.6
4.5	0.142	0.105	30.4
9	0.144	0.106	30.1
13.5	0.149	0.110	29.1
18	0.151	0.113	22.3
22.5	0.154	0.116	17.4
27	0.159	0.119	16.9
31.5	0.164	0.123	12.9

Figure 8. (Continued.)

through nonideal contact (ohmic) or lower site-access (kinetic, Fig. 6d).

Growing kinetic loss was the primary source of decreasing cell performance during extended operation of MEAs formed with different solid concentrations. Cell performance losses grew at higher solid concentration from 3.2 to 5.2 μV cycle^{-1} (at 5 mg$_{Ir}$ ml^{-1}) due to both higher kinetic and ohmic loss (HFR increased from 139 to 173 mΩ cm^2 at 5 mg$_{Ir}$ ml^{-1}, Figs. 4e–4i). At face value, the performance loss rate and loss mode (kinetic/ohmic) of MEAs sprayed with high solid concentrations was similar to high ionomer contents. With high solid concentration, however, the losses were comparatively more ohmic (HFR increased from 132 to 156 mΩ cm^2 at 0.8 mg$_{Nafion}$ mg$_{Ir}^{-1}$) than kinetic. These results suggest that different catalyst layer and interfacial deficiencies impact cell performance and durability in different ways, and that the separation of losses can be useful for diagnostics and to improve catalyst integration. Catalyst layer nonuniformities resulted in higher ohmic losses that disproportionally grew in ASTs, potentially due to catalyst layer degradation accentuating those nonuniformities. In contrast, high ionomer content resulted in higher kinetic losses that disproportionally grew in ASTs, potentially due to lower site-access initially limiting a delay in kinetic loss (Fig. 3c).

While large differences were found in ohmic/kinetic loss with different ink compositions, ex situ microscopy showed similar outcomes and relatively subtle differences in the anode catalyst layer following ASTs (Fig. 7). For each of the MEAs examined (optimum, high ionomer, high concentration, solvent ratio), significant bare patches in the catalyst layer were not found, suggesting that the complete dissolution of the catalyst layer was not needed for large performance losses to occur. Isolated instances of catalyst layer/membrane interfacial tearing were also found and may partially account for higher ohmic loss following ASTs by adding contact resistances. Additionally, migration of the anode catalyst into the membrane occurred. This was expected due to the elevated anode potential during operation and consistent with previous studies.[35,43]

Following studies on the ionomer content and the solid concentration in Ir-anode catalyst layer inks, the solvent ratio was tuned using water and n-propyl alcohol. In terms of initial performance nonidealities, the solvent ratio combined aspects of the ionomer and concentration experiments (kinetic/ohmic, catalyst/ionomer uniformity). The solvent ratio has an obvious impact on the evaporation rate during the coating process.[44] At alcohol-rich to even ratios (0.25–0.5 ml$_{Water}$ ml$_{nPA}^{-1}$), optimal performance was achieved and the performance differences were relatively small (Fig. 8a). In water-rich inks, however, performance decreases were observed due to a combination of slower kinetics and higher ohmic losses (Fig. 8b). Kinetic differences between the MEAs were present but relatively small, and consistent with small differences in capacitances (cyclic voltammograms) and polarization resistances (impedance spectra, Figs. 8c, 8d). Ohmic differences, however, tended to be larger and the HFR increased from 121 (0.33 ml$_{Water}$ ml$_{nPA}^{-1}$) to 139 mΩ cm^2 (1 ml$_{Water}$ ml$_{nPA}^{-1}$, Fig. 8d).

The solvent ratio had a measurable impact on the morphology of the sprayed catalyst layer. Water-rich to water-only inks produced catalyst layer nonuniformities that were apparent visually during the coating process, where the ink did not completely dry with each pass of the spray head. The spray velocity appeared to force the ink slightly wide of the head path and the majority of the ink dried in bands to either side. After spray completion, the nonuniformity was confirmed with XRF mapping, where the Ir loading (0.098 ± 0.017 mg$_{Ir}$ cm^{-2}) had minimum and maximum values of 0.067 and 0.144 mg$_{Ir}$ cm^{-2} (Fig. 8e). In HAADF-STEM images, nonuniformities were also observed (200 to 900 nm over a short span, 6 μm)
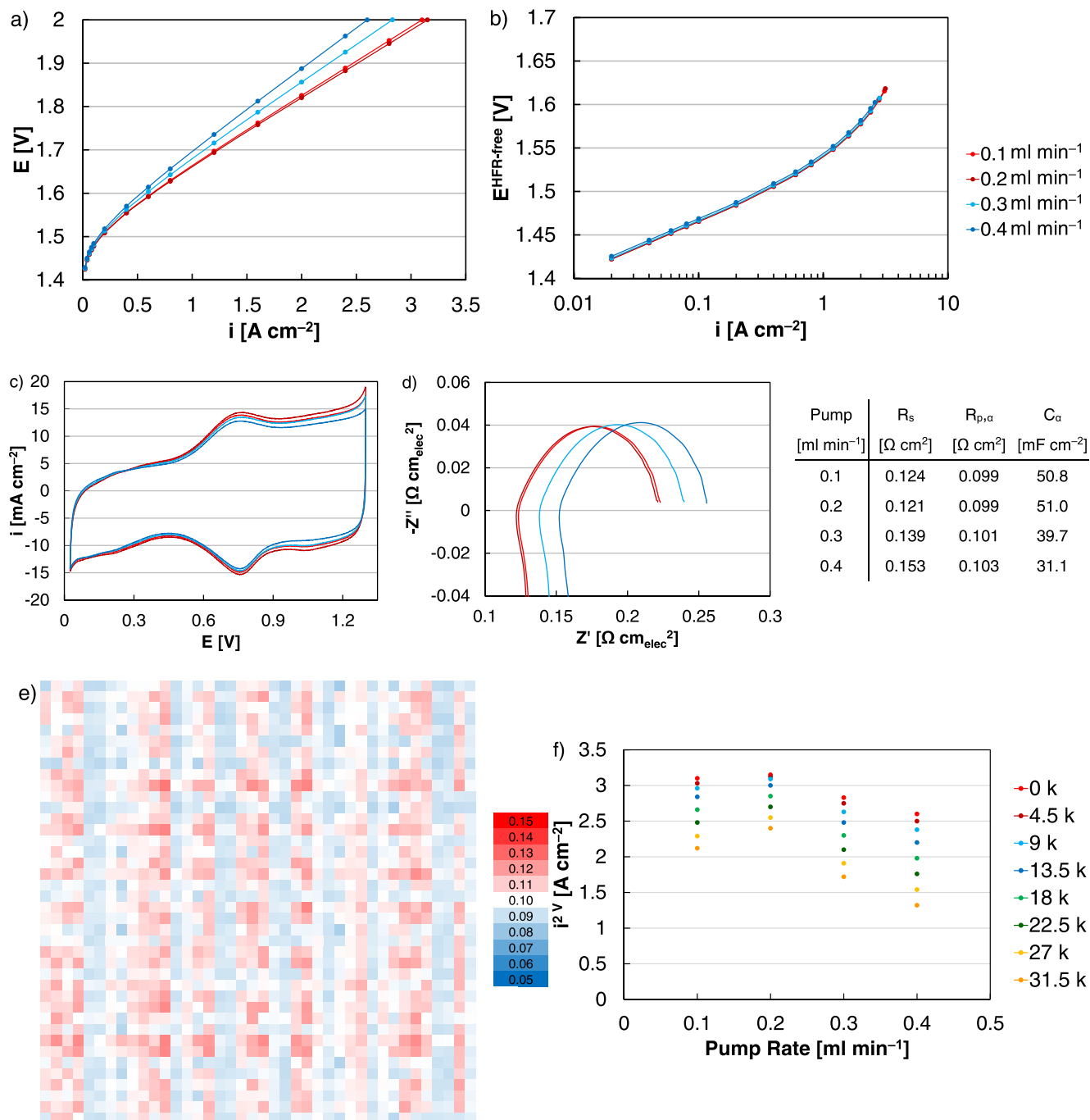
Figure 9. (a) Polarization curves, (b) HFR-corrected Tafel plots, (c) cyclic voltammograms, and (d) impedance spectra of MEAs sprayed while varying the pump rate in the anode catalyst layer ink at beginning of life. (e) XRF mapping of MEAs sprayed with a pump rate of 0.4 ml min^{-1} in the anode catalyst layer ink. (f) Current density at 2 V as a function of AST cycle count for MEAs sprayed with different pump rates for the anode catalyst layer. (f) Polarization curves, (g) HFR-corrected Tafel plots, (h) cyclic voltammograms, and (i) impedance spectra of MEAs sprayed with a pump rate for the anode catalyst layer of 0.4 ml min^{-1} as a function of AST cycle count. MEAs consisted of Ir oxide anodes and Pt/HSC cathodes with loadings of 0.1 mg$_{Ir,Pt}$ cm^{-2}, and were operated at 80 °C.

that were similar albeit slightly more regular than catalyst layers formed with high solid concentration (Fig. 5e). While the average layer thicknesses appeared roughly similar to the optimum, thinner portions may suggest differences in porosity. Additionally, a higher frequency of Ir aggregates was found (denser sections, higher contrast), and may indicate that water-heavy inks and longer drying times allow for ink segregation and Ir flocculation (Fig. 5e).[44] STEM-EDS analysis of the water-heavy catalyst layer also confirmed less-than-ideal catalyst-ionomer integration (Fig. 6d), with more high contrast fluorine regions suggesting poor dispersion. There was also a higher frequency of regions devoid of ionomer

which may have resulted in lower site-access and accounted for the lower exchange current density initially. In this sense, water-rich inks created suboptimal uniformities in both the catalyst layer thickness and ionomer integration, which produced kinetic and ohmic loss and combined aspects from both the ionomer content (primarily kinetic) and solid concentration (primarily ohmic) experiments.

In durability testing, the performance loss rate varied from 3.2 (0.33 ml$_{Water}$:ml$_{nPA}$) to 6.7 μV cycle^{-1} (water-only), and of the ink parameters evaluated, the solvent ratio produced a comparatively large variation in MEA durability (Fig. 8f). While AST losses were
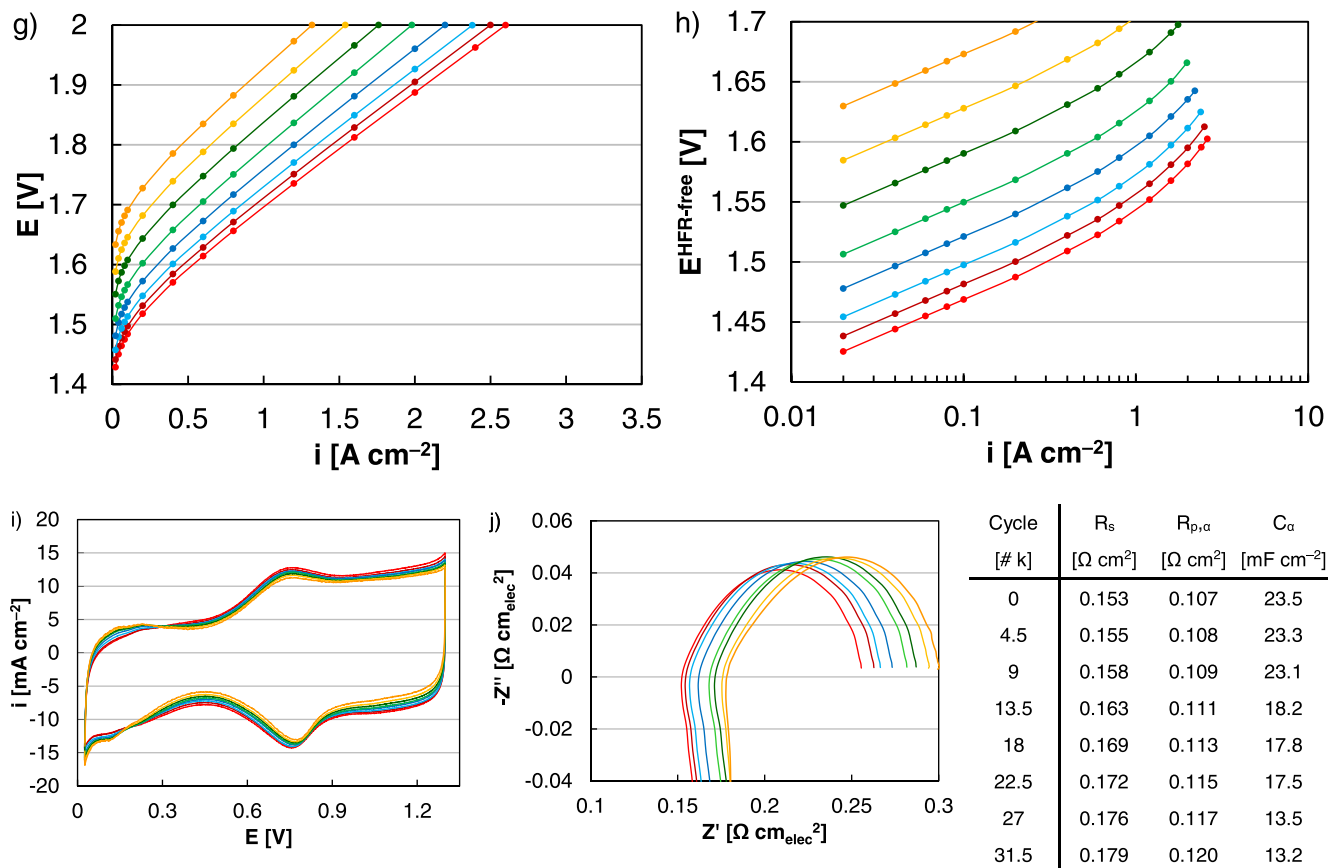
Cycle	R_s	$R_{p,\alpha}$	C_α
[# k]	[Ω cm^2]	[Ω cm^2]	[mF cm^{-2}]
0	0.153	0.107	23.5
4.5	0.155	0.108	23.3
9	0.158	0.109	23.1
13.5	0.163	0.111	18.2
18	0.169	0.113	17.8
22.5	0.172	0.115	17.5
27	0.176	0.117	13.5
31.5	0.179	0.120	13.2

Figure 9. (Continued.)

primarily kinetic, water-rich and water-only inks produced MEAs with both larger kinetic and ohmic losses. Catalyst layer differences may account for the higher loss rates. As with the ionomer content experiments, suboptimal catalyst-ionomer integration may isolate Ir sites, resulting in lower site-access and kinetics initially, and higher losses in ASTs by minimizing any delay in kinetic loss. Kinetic deterioration was found in polarization curves and was consistent with decreasing exchange current densities, thinning capacitance (cyclic voltammograms), and growing polarization resistances (impedance spectra, Figs. 8g–8j). As with the solid concentration experiments, suboptimal catalyst layer uniformity may add small resistances due to a reduced catalyst-PTL interfacial contact. ASTs may further accentuate those nonuniformities and higher ohmic loss was consistent with growing interaction with the Pt-PTL coating (cyclic voltammograms, hydrogen underpotential deposition) and HFR values (water-only, 139 to 164 mΩ cm^2, Figs. 8i, 8j). Ex situ microscopy of the catalyst layers formed with water-heavy inks after ASTs showed similar trends to other ink compositions, where Ir migrated into the membrane and instances of catalyst layer/membrane interfacial tearing were found (Fig. 7).

Spray parameters.—In addition to tuning ink variables, spray parameters were modified to evaluate their effect on performance and durability. Changing the pump rate, or how quickly the ink was sprayed onto the membrane, affected the time required to spray CCMs from 24 (0.4 ml min^{-1}) to 94 min (0.1 ml min^{-1}, 4 × 25 cm^2). At very low rates (0.1 ml min^{-1}), slight Ir agglomeration appeared in the spray line; although ink aggregation can impact catalyst layer properties, only small differences in kinetics and ohmic loss were found compared to the optimum and the low spray rate may not have been low enough to observe larger differences. Additionally, the pump rate affected the ink drying time and higher spray rates

(0.3–0.4 ml min^{-1}) caused ink pooling on the spray bed that resulted in higher variability in the catalyst loading. At a high pump rate (0.4 ml min^{-1}), minimal differences were seen in kinetics and lower performance was primarily due to higher ohmic loss (121 to 153 mΩ cm^2, Figs. 9a–9d). The higher ohmic loss may indicate that increasing the pump rate resulted in less uniform catalyst layers but with reasonable catalyst-ionomer integration. High pump rates maintained kinetic performance, confirmed with high exchange current densities and supported by slight differences in capacitance (cyclic voltammograms) and polarization resistances (impedance spectra). The anticipated catalyst layer nonuniformities were confirmed with XRF mapping (0.100 ± 0.009 mg$_{Ir}$ cm^{-2}) where the maximum and minimum loadings were 0.123 and 0.080 mg$_{Ir}$ cm^{-2} respectively (Fig. 9e). In durability testing, the performance loss rate varied from 3.2 to 7.5 μV h^{-1} (Fig. 9f). Consistent trends were found, where the loss was primarily kinetic and similar kinetic losses were found with changes to the pump rate. At high pump rates, however, higher transport and ohmic loss were found (Figs. 9g–9j). The increasing ohmic losses were likely due to catalyst layer nonuniformities initially that were accentuated by ASTs, resulting in increased Pt-PTL coating interaction and higher HFR values.

Finally, the temperature of the spray bed was varied, where the bed temperature impacted the drying time once the ink contacted the membrane. At lower temperature, differences from the optimum performance were due to a combination of lower kinetics and higher ohmic loss (Figs. 10a, 10b). Increased kinetic loss suggests that the catalyst-ionomer integration may not have been ideal, and slightly thinner capacitances (cyclic voltammograms) and higher polarization resistances (0.107 Ω cm^2) were observed (Figs. 10c, 10d). Lower bed temperature also appeared to cause some ink pooling on the spray bed and resulted in higher catalyst loading variability (0.103 ± 0.015 mg$_{Ir}$ cm^{-2} from XRF mapping, with maximum and

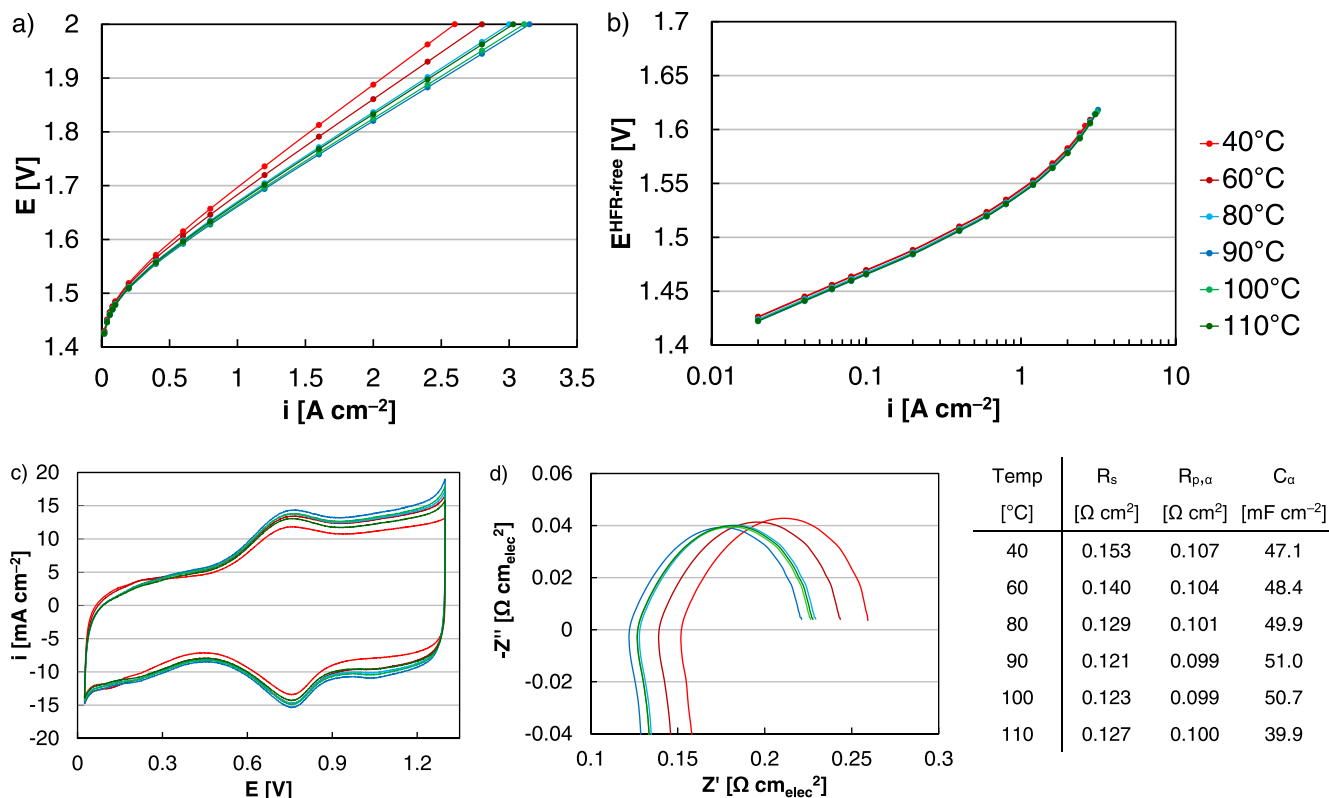| Temp	R_s	$R_{p,\alpha}$	C_α
[°C]	[Ω cm^2]	[Ω cm^2]	[mF cm^{-2}]
40	0.153	0.107	47.1
60	0.140	0.104	48.4
80	0.129	0.101	49.9
90	0.121	0.099	51.0
100	0.123	0.099	50.7
110	0.127	0.100	39.9

Figure 10. (a) Polarization curves, (b) HFR-corrected Tafel plots, (c) cyclic voltammograms, and (d) impedance spectra of MEAs sprayed while varying the drying temperature for the anode catalyst layer at beginning of life. (e) XRF mapping of MEAs sprayed with a drying temperature of 40 °C in the anode catalyst layer. (f) Current density at 2 V as a function of AST cycle count for MEAs sprayed with different drying temperatures for the anode catalyst layer. (f) Polarization curves, (g) HFR-corrected Tafel plots, (h) cyclic voltammograms, and (i) impedance spectra of MEAs with a drying temperature in the anode catalyst layer of 40 °C as a function of AST cycle count. MEAs consisted of Ir oxide anodes and Pt/HSC cathodes with loadings of 0.1 mg$_{Ir,Pt}$ cm^{-2}, and were operated at 80 °C.

minimum values of 0.153 and 0.067 mg$_{Ir}$ cm^{-2}) and higher HFR values (153 mΩ cm^2 at 40 °C, Figs. 10d, 10e). At higher temperature, minimal changes to kinetics and a slight increase in ohmic loss were found (HFR 127 mΩ cm^2 at 110 °C). While small HFR increases may have been due to differences in the catalyst layer, it was also possible that membrane changes occurred at elevated temperature over extended periods of time and some coloring was observed (orange tinting). In terms of durability, the performance loss was primarily kinetic and varied from 3.2 to 8.2 μV h^{-1}, the largest range of any parameter evaluated (Fig. 10f). At a low bed temperature (40 °C) the kinetic losses were significantly larger, potentially due to poor catalyst-ionomer integration and limited Ir site access initially that exacerbated kinetic losses over time; these losses were further accompanied by thinning capacitance (cyclic voltammograms) and growing polarization resistances (Figs. 10g–10j). Higher degrees of ohmic loss were also found, confirmed with increasing HFR values (153 to 183 mΩ cm^2) and supported by higher Pt-PTL coating participation (cyclic voltammograms, hydrogen underpotential deposition). Higher ohmic losses were potentially due to less uniform catalyst layers initially that were accentuated in ASTs during Ir dissolution and catalyst layer thinning.

Figure 11 summarizes the overarching trends in MEA performance and durability arising from both ink variables (ionomer content, solid concentration, solvent ratio) and spray parameters (pump rate, drying temperature). When separating losses in polarization curves, kinetic and ohmic loss were the primary sources of nonideal performance (Fig. 11a). Additionally, ASTs produced large kinetic losses, where the exchange current density decreased 2–3 orders of magnitude and added 100–200 mV in overpotential

(at 1.2 A cm^{-2}, Figs. 11b, 11c). Secondarily, ASTs resulted in ohmic loss, where the HFR increased 10–35 mΩ cm^2 and added 10–60 mV in overpotential (at 1.2 A cm^{-2}, larger at higher current density, Figs. 11b, 11c). Although the kinetic and ohmic loss rate varied, two takeaways were consistent. First, lower performance initially tended to result in higher durability losses and speaks to the need to establish robust baselines in electrolysis performance and durability, and to optimize catalyst layer integration to fully realize component improvements. Second, when separating kinetic and ohmic losses, lower kinetics initially accelerated kinetic loss and higher HFR values accelerated HFR increases in ASTs. Nonideal performance tended to correlate to catalyst-ionomer segregation and catalyst layer nonuniformities, and ASTs may accentuate these catalyst layer deficiencies and performance losses. Although ink and spray variables are interconnected and did not exclusively affect a single loss mechanism, poor catalyst-ionomer integration and catalyst layer uniformity tended to have greater impacts on kinetic and ohmic loss, respectively. Separating these losses in initial performance and quantifying how these losses change during extended operation may therefore be useful as a diagnostics approach to elucidate why suboptimal performance/durability occurred and how catalyst layer modifications could improve performance/durability.

Conclusions

Several ink and spray parameters were evaluated in this study, including the ionomer content, solid concentration, solvent ratio, pump rate, and drying temperature. When comparing individual variables some commonalities were observed, where changes to ink composition or spray parameters resulted in similar changes to the
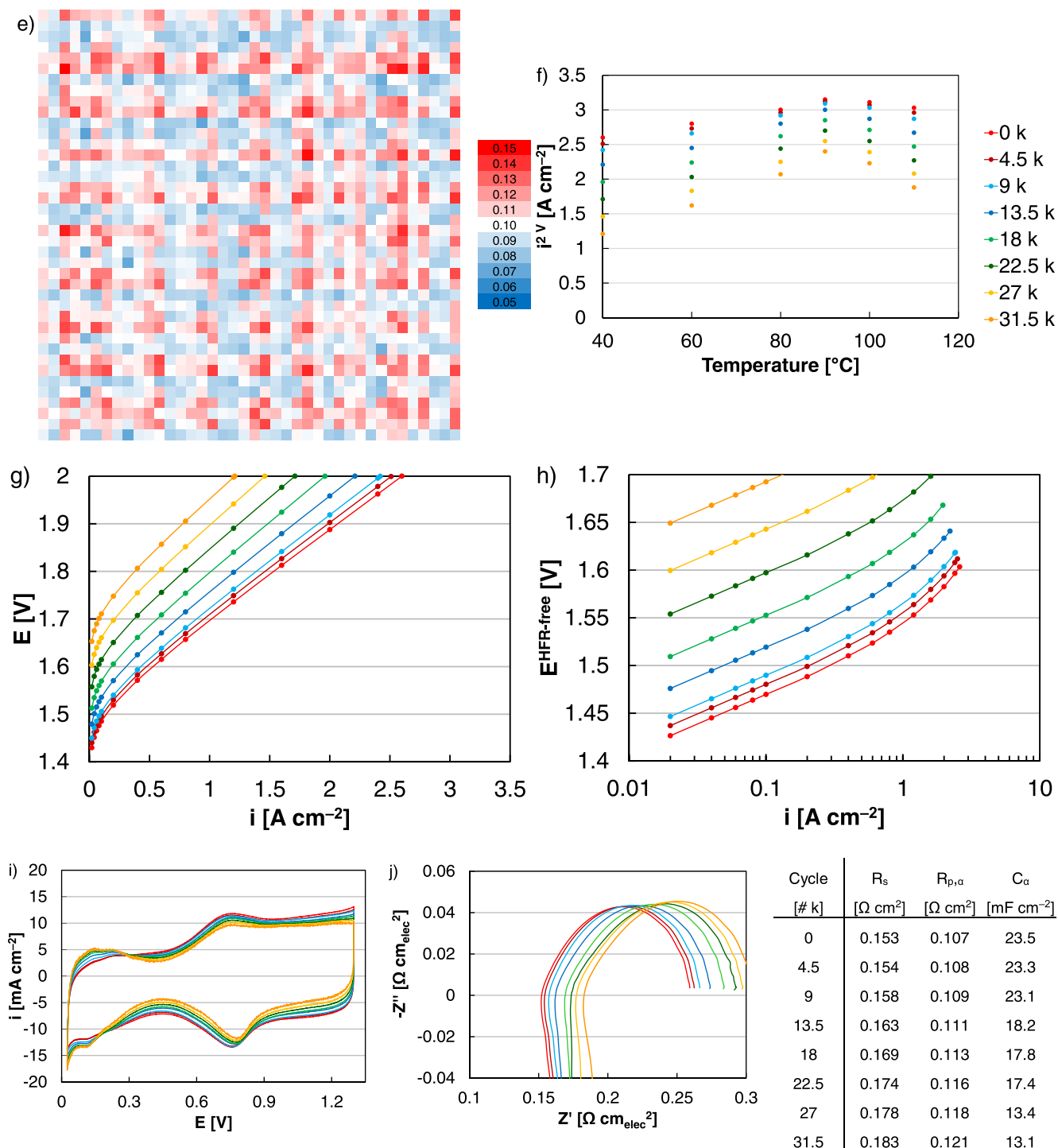
Cycle	R_s	$R_{p,\alpha}$	C_α
[# k]	[Ω cm^2]	[Ω cm^2]	[mF cm^{-2}]
0	0.153	0.107	23.5
4.5	0.154	0.108	23.3
9	0.158	0.109	23.1
13.5	0.163	0.111	18.2
18	0.169	0.113	17.8
22.5	0.174	0.116	17.4
27	0.178	0.118	13.4
31.5	0.183	0.121	13.1

Figure 10. (Continued.)

catalyst layer and affected cell-level performance and durability in similar ways. First, modifications to the ionomer quantity or dispersion largely affected kinetic performance. Excess ionomer and poor incorporation (catalyst-ionomer segregation) resulted in slower kinetics, likely due to the ionomer limiting access to Ir sites. Extended operation of these MEAs accelerated kinetic loss, potentially due to lower site-access initially limiting any delays in kinetic loss. Second, nonuniformities in the catalyst layer thickness adversely impacted ohmic loss, potentially by creating poor catalyst layer-PTL contact and adding contact resistances. ASTs also accelerated these losses, potentially by accentuating catalyst layer nonuniformities (ohmic/transport) and resulted in increased access to the Pt-PTL coating.

Efforts to understand catalyst layer formation and the impact of catalyst layer properties on electrolyzer performance and durability are critical to creating robust baselines for component developments to build upon. While sprayed electrodes tend to focus on fundamental science, the properties of optimal MEAs (uniform catalyst layers, ionomer content, catalyst-ionomer integration) can translate to manufacturing-relevant processes. Differences in kinetic/ohmic
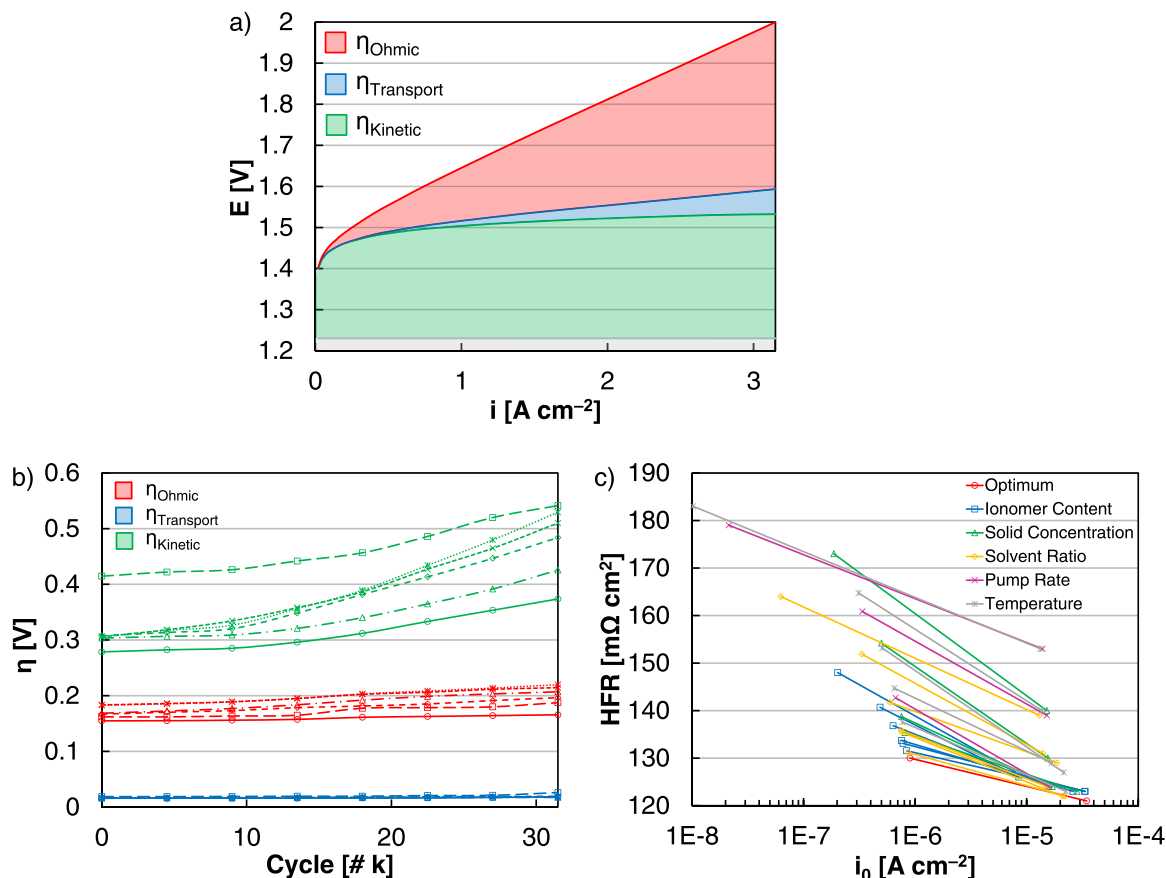
Figure 11. (a) Polarization curve of optimum ink with losses separated into ohmic (red), transport (blue), and kinetic (green). (b) Overpotential, separated into ohmic (red), transport (blue), and kinetic (green) loss, at 1.2 A cm^{-2}. Data included for the optimum ($\bigcirc$), high ionomer content (0.8 mg$_{Nafion}$ mg$_{Ir}^{-1}$, $\square$), high concentration (5 mg$_{Ir}$ ml^{-1}, $\triangle$), water-rich (1 ml$_{Water}$ ml$_{Ink}^{-1}$, $\lozenge$), high pump rate (0.4 ml min^{-1}, $\times$), and low temperature (40 °C, $*$) inks. (c) Exchange current density (x-axis, kinetic) and HFR value (y-axis, ohmic), initially (lower right) and following ASTs (upper left) for each MEA evaluated. Data included for the optimum ink (red) and ionomer content (blue), solid concentration (green), solvent ratio (yellow), pump rate (purple), and temperature (grey) experiments. MEAs consisted of Ir oxide anodes and Pt/HSC cathodes with loadings of 0.1 mg$_{Ir,Pt}$ cm^{-2}, and were operated at 80 °C.

performance and how those losses grow during extended operation can further provide insight and diagnose the cause of suboptimal performance from different processing techniques or conditions.

Commercial electrolyzers today typically avoid durability losses with a constant load (power input) and high catalyst loadings. An improved understanding of durability will be needed in the future, however, as low temperature electrolysis shifts towards low-cost applications and load following variable power sources. This works demonstrates that while improving upon individual component performance and durability is critical, further studies optimizing MEA integration are also sorely needed to fully realize the potential of novel components and manufacturing processes. Understanding how these factors affect performance and durability losses are necessary to reduce the production cost of hydrogen and increase electrolysis implementation.

ORCID

Shaun M. Alia https://orcid.org/0000-0002-7647-9383
David A. Cullen https://orcid.org/0000-0002-2593-7866

References

1. B. Pivovar, N. Rustagi, and S. Satyapal, *The Electrochemical Society Interface*, **27**, 47 (2018).
2. B. Pivovar, "H2 at Scale." *NREL Workshop* (U. S. Department of Energy Editor) (2016), https://www.energy.gov/sites/prod/files/2016/12/f34/fcto_h2atscale_work-shop_pivovar_2.pdf.
3. DOE H2A Production Analysis, *U.S. Department of Energy Office of Energy Efficiency and Renewable Energy* (2018), https://hydrogen.energy.gov/h2a-delivery.html.
4. U. Babic, M. Suermann, F. N. Büchi, L. Gubler, and T. J. Schmidt, *J. Electrochem. Soc.*, **164**, F387 (2017).
5. K. Ayers, N. Danilovic, R. Ouimet, M. Carmo, B. Pivovar, and M. Bornstein, *Annual review of chemical and biomolecular Engineering*, **10**, 219 (2019).
6. K. Ayers, *Current Opinion in Electrochemistry*, **18**, 9 (2019).
7. S. A. Grigoriev, K. A. Dzhus, D. G. Bessarabov, and P. Millet, *Int. J. Hydrogen Energy*, **39**, 20440 (2014).
8. A. Weiß, A. Siebel, M. Bernt, T.-H. Shen, V. Tileli, and H. Gasteiger, *J. Electrochem. Soc.*, **166**, F487 (2019).
9. S. M. Alia, S. Stariha, and R. L. Borup, *J. Electrochem. Soc.*, **166**, F1164 (2019).
10. U. Babic, M. Tarik, T. J. Schmidt, and L. Gubler, *J. Power Sources*, **451**, 227778 (2020).
11. T. Schuler, T. J. Schmidt, and F. N. Büchi, *J. Electrochem. Soc.*, **166**, F555 (2019).

12. C. Rakousky, G. P. Keeley, K. Wippermann, M. Carmo, and D. Stolten, *Electrochim. Acta*, **278**, 324 (2018).
13. C. Liu, M. Carmo, G. Bender, A. Everwand, T. Lickert, J. L. Young, T. Smolinka, D. Stolten, and W. Lehnert, *Electrochem. Commun.*, **97**, 96 (2018).
14. H.-Y. Jung, S.-Y. Huang, P. Ganesan, and B. N. Popov, *J. Power Sources*, **194**, 972 (2009).
15. C. Rakousky, U. Reimer, K. Wippermann, M. Carmo, W. Lueke, and D. Stolten, *J. Power Sources*, **326**, 120 (2016).
16. T. Reier, M. Oezaslan, and P. Strasser, *ACS Catal.*, **2**, 1765 (2012).
17. N. Danilovic, R. Subbaraman, K.-C. Chang, S. H. Chang, Y. J. Kang, J. Snyder, A. P. Paulikas, D. Strmcnik, Y.-T. Kim, and D. Myers, *The Journal of Physical Chemistry Letters*, **5**, 2474 (2014).
18. M. Pourbaix, *Atlas of Electrochemical Equilibria in Aqueous Solutions* (National Association of Corrosion Engineers, Houston, Texas) (1974).
19. K. Ayers, *High Efficiency Pem Water Electrolysis Enabled by Advanced Catalysts, Membranes and processes* (2019), https://hydrogen.energy.gov/pdfs/review19/p155_ayers_2019_o.pdf.
20. H. Xu, *High-Performance, Long-Lifetime Catalysts for Proton Exchange Membrane Electrolysis* (2017), https://hydrogen.energy.gov/pdfs/review17/pd103_xu_2017_o.pdf.
21. S. M. Alia and G. C. Anderson, *J. Electrochem. Soc.*, **166**, F282 (2019).
22. S. M. Alia, M.-A. Ha, G. C. Anderson, C. Ngo, S. Pylypenko, and R. E. Larsen, *J. Electrochem. Soc.*, **166**, F1243 (2019).
23. S. M. Alia, B. Rasimick, C. Ngo, K. Neyerlin, S. S. Kocha, S. Pylypenko, H. Xu, and B. S. Pivovar, *J. Electrochem. Soc.*, **163**, F3105 (2016).
24. K. A. Lewinski, D. van der Vliet, and S. M. Luopa, *ECS Trans.*, **69**, 893 (2015).
25. S. Zhao, A. Stocks, B. Rasimick, K. More, and H. Xu, *J. Electrochem. Soc.*, **165**, F82 (2018).
26. K. E. Ayers, J. N. Renner, N. Danilovic, J. X. Wang, Y. Zhang, R. Maric, and H. Yu, *Catal. Today*, **262**, 121 (2016).
27. M. Suermann, B. Bensmann, and R. Hanke-Rauschenbach, *J. Electrochem. Soc.*, **166**, F645 (2019).
28. C. Rakousky, U. Reimer, K. Wippermann, S. Kuhri, M. Carmo, W. Lueke, and D. Stolten, *J. Power Sources*, **342**, 38 (2017).
29. K. E. Ayers, E. B. Anderson, C. Capuano, B. Carter, L. Dalton, G. Hanlon, J. Manco, and M. Niedzwiecki, *ECS Trans.*, **33**, 3 (2010).
30. D. Bessarabov, A. Kruger, S. M. Luopa, J. Park, A. A. Molnar, and K. A. Lewinski, *ECS Trans.*, **75**, 1165 (2016).
31. M. Hamdan, *Electrochemical Compression* (2017), https://hydrogen.energy.gov/pdfs/review17/pd136_hamdan_2017_o.pdf.
32. G. Wei, Y. Wang, C. Huang, Q. Gao, Z. Wang, and L. Xu, *Int. J. Hydrogen Energy*, **35**, 3951 (2010).
33. U. Babic, T. J. Schmidt, and L. Gubler, *J. Electrochem. Soc.*, **165**, J3016 (2018).
34. Z. Kang et al., *Nano Energy*, **47**, 434 (2018).
35. S. M. Alia, *H2@Scale: Experimental Characterization of Durability of Advanced ElectrolyzerConcepts in Dynamic Loading* (2019), https://hydrogen.energy.gov/pdfs/review19/ta022_alia_2019_o.pdf.
36. K. Ayers, *High Efficiency PEM Water Electrolysis Enabled by Advanced Catalysts, Membranes and Processes* (2020), https://hydrogen.energy.gov/pdfs/review20/p155_ayers_2020_p.pdf.
37. S. M. Alia, K. E. Hurst, S. S. Kocha, and B. S. Pivovar, *J. Electrochem. Soc.*, **163**, F3051 (2016).
38. R. Cottis and S. Turgoose, *Electrochemical Impedance and Noise* (National Association of Corrosion Engineers, Houston, Texas) (1999).
39. X. Tan, J. Shen, N. Semagina, and M. Secanell, *J. Catal.*, **371**, 57 (2019).
40. F. Mansfeld, *Analysis and Interpretation of EIS Data for Metals and Alloys* (Technical Report, Solartron-Schlumberger Editor, Hamshire, England) (1993).
41. S. M. Alia, *H2@Scale: Experimental Characterization of Advanced ElectrolyzerConcepts in Dynamic Loading* (2018), https://hydrogen.energy.gov/pdfs/review18/tv146_alia_2018_p.pdf.
42. P. Trinke, G. P. Keeley, M. Carmo, B. Bensmann, and R. Hanke-Rauschenbach, *J. Electrochem. Soc.*, **166**, F465 (2019).
43. H. Xu, *High-Performance, Long-Lifetime Catalysts for Proton Exchange Membrane Electrolysis* (2015), http://hydrogen.energy.gov/pdfs/review15/pd103_xu_2015_o.pdf.
44. S. Khandavalli, J. H. Park, N. N. Kariuki, S. F. Zaccarine, S. Pylypenko, D. J. Myers, M. Ulsh, and S. A. Mauger, *ACS Applied Materials & Interfaces*, **11**, 45068 (2019).